PHYSICAL REVIEW B **88**, 035128 (2013)

Tuning the quantum oscillations of surface Dirac electrons in the topological insulator Bi_2Te_2Se by liquid gating

Jun Xiong,[1] Yuehaw Khoo,[1] Shuang Jia,[2] R. J. Cava,[2] and N. P. Ong[1]
[1]*Department of Physics, Princeton University, Princeton, New Jersey 08544, USA*
[2]*Department of Chemistry, Princeton University, Princeton, New Jersey 08544, USA*
(Received 9 October 2012; revised manuscript received 28 June 2013; published 22 July 2013)

In Bi_2Te_2Se, the period of quantum oscillations arising from surface Dirac fermions can be increased sixfold using ionic liquid gating. At high gate voltages, the Fermi energy reaches the $N = 1$ Landau level in a 14-T field. This enables the $\frac{1}{2}$ shift predicted for the Dirac spectrum to be measured accurately. A surprising result is that liquid gating strongly enhances the surface mobility. By analyzing the Hall conductivity, we show that the enhancement occurs on only one surface. We present evidence that the gating process is fully reversible (hence consistent with band bending by the E field from the anion layer accumulated). In addition to the surface carriers, the experiment yields the mobility and density of the bulk carriers in the impurity band. By analyzing the charge accumulation vs gate voltage, we also obtain estimates of the depletion width and the areal depletion capacitance C_d/A. The value of C_d/A implies an enhanced electronic polarizability in the depletion region.

DOI: 10.1103/PhysRevB.88.035128 PACS number(s): 71.70.Ej, 72.15.Rn, 03.65.Vf, 73.25.+i

I. INTRODUCTION

A topological insulator (TI) is characterized by the existence of current-carrying surface states that traverse the bulk energy gap.[1,2] There is strong interest in the helical nature of the surface states, which results from the locking of the electron's spin transverse to its momentum. In bismuth-based TI materials, photoemission spectroscopy[3] and scanning tunneling microscopy (STM)[4] have confirmed the spin-locking feature. In transport experiments, the surface states have been detected by surface Shubnikov–de Haas (SdH) oscillations in Bi_2Te_3[5] and $(Bi,Sb)_2Se_3$[6] and by Aharonov-Bohm oscillations in Bi_2Se_3 nanowires.[7]

Among Bi-based TI materials, Bi_2Te_2Se currently displays the highest bulk resistivities ($\rho = 1$–$6\ \Omega$cm at 4 K).[8–11] Despite the large ρ, SdH oscillations may be tracked to temperatures T as high as 38 K.[9] A persistent problem, however, is that the surface Fermi energy E_F in as-grown crystals is still quite high (∼200 meV above the Dirac point). An *in situ* method that demonstrably tunes E_F would greatly facilitate experiments at the Dirac point, as proposed in Refs. 1 and 2. Several groups have applied conventional electrostatic gating to tune the chemical potential μ in exfoliated crystals[12–14] and in thin-film samples of Bi_2Se_3.[15] The newer technique of liquid gating has also been used on Bi-based materials.[16–20] However, in these experiments, SdH oscillations were either not detected or poorly resolved[14] even if the second derivative is used. Tuning the quantum oscillations and showing that they arise from surface Dirac electrons remain to be accomplished.

Here we report that the surface SdH oscillations in Bi_2Te_2Se can be tuned over a broad range using an ionic liquid (DEME-TFSI). In lowering E_F substantially, we access the $N = 1$ Landau level (LL) in a magnetic field $B = 14$ T. This allows the $\frac{1}{2}$ shift characteristic of Dirac electrons to be measured with greatly improved resolution. We find that the intercept remains fixed at $\frac{1}{2}$ even as the surface density is tuned by factors of 3–6. An unexpected finding is that liquid gating leads to strong enhancement of the mobility μ_s of the surface carriers. We attribute the enhancement to the "smoothing" of local potential fluctuations seen by Dirac fermions. Aside from moving E_F closer to the Dirac point, the tunability yields direct information on the surface and bulk conduction. The additional information enables us to determine how the surface and bulk mobilities change with the gate voltage V_G. We discuss the evidence that the liquid gating in our experiment is causing band bending rather than unwanted chemical reaction. Finally, thanks to the SdH oscillations, we can measure five parameters at each setting of V_G (E_F and μ_s of the surface carriers, the bulk density and mobility, and the total ionic charge Q deposited). The five parameters provide cross-checks for the gating experiment. In particular, we determine the depletion capacitance C_d, which measures the polarizability of the depletion region.

As reported earlier,[8,9,11] the resistance $R(T)$ in Bi_2Te_2Se rises monotonically to very large values as $T \to 4$ K [curve at $V_G = 0$ in Fig. 1(a)]. Analysis of the Hall coefficient R_H at 5 K [Fig. 1(b)] reveals a population of bulk n-type carriers much higher than the population of surface electrons. Nonetheless, a modest, negative gate voltage V_G can increase R by 40% [Fig. 1(a)] and $|R_H|$ by a factor of 2 at 5 K [Fig. l(b)]. V_G is applied to the gold electrode [inset in Fig. 1(a)] at 220 K, and the sample is then cooled below the liquid's glass transition. After the low-T measurements are completed, the sample is warmed to 220 K (at 2 K/min) and V_G is reset. The "gating" temperature is selected within the optimal window 220–240 K (see below and Appendix A). At 4 K, the large E field induced by the surface anion charge Q (1–$4 \times 10^{14} e$ cm^{-2}) creates a depletion layer that penetrates deep into the bulk (5–20 μm), where e is the electron charge. As shown in the inset in Fig. 1(b), the induced upward bending of the bands decreases E_F.

At each value of V_G, the curves of R vs B display SdH oscillations. To focus on the SdH signal, we have subtracted off a smooth background ρ_B to isolate the oscillatory part of the resistance, $\Delta\rho_{xx} \equiv \rho_{xx} - \rho_B$. Figure 3(a) displays plots of $\Delta\rho_{xx}$ in sample 1 versus $1/B$ for 5 values of V_G. The period of the SdH oscillations increases monotonically as V_G changes from 0 to −4.2 V, in accordance with our expectation that E_F is decreasing. Surprisingly, the SdH amplitude is strongly

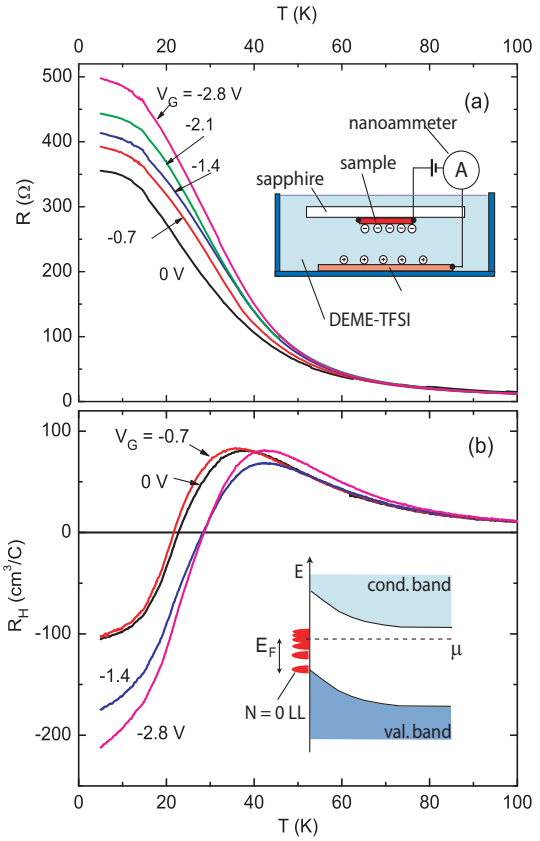

FIG. 1. (Color online) Resistance R per square (a) and Hall coefficient R_H vs T (b) in Bi_2Te_2Se at selected V_G in sample 1. R_H is measured at fixed B (3 T). Changing V_G from 0 to -2.8 V increases R by 40% and $|R_H|$ by 2×. Inset in (a): Cell housing the sample and the ionic liquid DEME-TFSI. The Au electrode (a circular plate of radius 1.5 mm) is separated from the sample by 0.5 mm. Inset in (b): Sketch of the band bending induced by liquid gating. Negative ions deposited on the crystal leads to upward band bending. At the surface, this causes E_F to decrease towards the Dirac point. LLs are shown as filled half-ovals.

enhanced between $V_G = 0$ and $V_G = -2.1$ V (the former is shown amplified by 5×). Dotted curves are the best fits[11] to the Lifshitz-Kosevich expression for SdH oscillations using only one frequency component. From the fits, we may infer how the surface mobility μ_s changes with V_G (see below). The same trends are evident in sample 2, which has a higher starting surface density n_s but is taken to $B = 45$ T [Fig. 3(b)]. We find that the SdH oscillations are not resolved at $V_G = 0$ but become prominent at $V_G = -1.5$ V.

II. EXPERIMENTAL DETAILS

In our experiment, the sample is immersed in the ionic liquid DEME-TFSI, comprised of cations $(CH_3CH_2)_2(CH_2CH_2OCH_3)CH_3N^+$ and anions $(CF_3SO_2)_2N^-$. The liquid is pumped at 25 °C for 2 h prior to application to minimize the water content. Liquid gating has several pitfalls when used on crystals. After the gate voltage V_G is selected at a "gating temperature" (Appendix A), the sample is cooled to 5 K for SdH measurements. The stresses induced by repeated freezing and thawing of the ionic liquid can snap the leads or the crystal itself. Also, a large $|V_G|$ can trigger an electrical discharge which invariably leads to a steep collapse of R (at 5 K). Unlike in thin films, changes to R with V_G are not resolved above ∼100 K [see Fig. 1(a)]. To minimize sample damage, we start at $V_G = 0$, followed by measurements at increasingly negative V_G until the sample fails (usually by a discharge event). At 220 K, V_G is changed in steps of -0.1 V, while monitoring the transient current $I_{\rm trans}$ (1-40 nA). The time spent at 220 K is typically 300–500 s. We emphasize that the changes to ρ and n_H are reversible (see below). Upon returning V_G to 0, we recover the same starting value of R (at 5 K) provided $|V_G|$ is kept below ∼2 V.

The crystal dimensions of sample 1 are $0.9 \times 0.75 \times 0.05$ mm^3. For sample 2, they are $1.35 \times 0.61 \times 0.026$ mm^3. In sample 2, the steepest change in μ_s occurs between $V_G = 0$ and $V_G = -1.5$ V, at which $\mu_s = 2800$ cm^2/V s. At a larger gate, it saturates ($\mu_s = 3000$ cm^2/V s at -6 V).

The possibility that the strong E field can induce chemical doping of the sample is an important concern in liquid-gating experiments. We note that the effects of chemical reaction are inherently nonreversible. In particular, let us assume that chemically induced doping occurs at some finite V_G leading to changes in ρ and n_H (measured when cooled to 4 K). When the sample is rewarmed to 240 K and V_G is reset to 0, we should not expect ρ and n_H to recover their starting values when recooled to 4 K (resetting V_G to 0 cannot reverse the chemical damage). Hence, we adopt the working assumption that the absence of resolvable hystereses in ρ and n_H (measured at 4 K) as V_G is cycled provides evidence that band bending is the dominant effect and chemical reaction effects are minimal. We have performed a much broader set of tests (on sample 3) to investigate details of the ion accumulation process over an extended range of gating temperatures ($208 < T < 260$ K). Samples 1 and 2, from which the detailed SdH results were obtained, were not subjected to these cycling processes, to minimize stress damage.

Figure 2 shows the variation of ρ [Fig. 2(a)] and n_H in sample 3 as V_G is changed stepwise from 0 to -1.3 V and back. After the V_G is set anew (at the gating $T = 240$ K), we wait for 800 s to accumulate anions before cooling to 4 K for the measurements of ρ and n_H. By monitoring the transient charging current $I_{\rm trans}$, we have also measured the ion accumulation charge $Q(t)$ (Appendix B). The absence of hysteresis, within the experimental uncertainty, is evidence that the changes are fully reversible and hence caused by band-bending effects. The experiment, repeated at 260 K, also shows negligible hysteresis.

Apart from chemical reaction, two other important factors are incomplete melting of the ionic charge configuration when T is too close to the glass transition and the intrinsic (activated) bulk conductance of the ionic liquid. These additional factors have been investigated using the measured $Q(t)$. We discuss them in Appendix A.

III. TUNING THE SURFACE DIRAC-STATE DENSITY

In finite B, the surface electronic states are quantized into LLs with quantum numbers $N = 0, 1, \ldots$. The index field B_n is the field at which E_F falls between two LLs. For Schrödinger states, the integer n counts the number of occupied

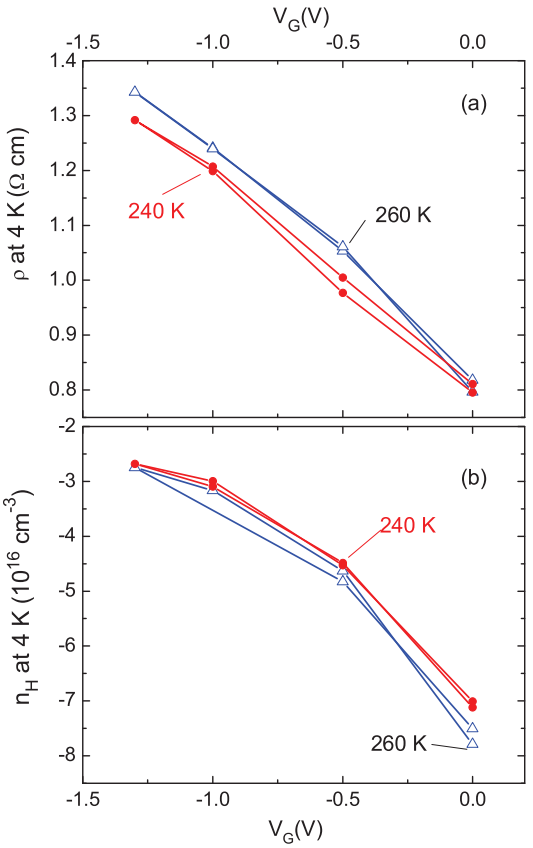

FIG. 2. (Color online) Test experiments to show negligible hysteresis in the sample's resistivity ρ (a) and Hall density n_H (b), as V_G is changed from 0 to -1.3 V, then back to 0 V at temperatures $T = 240$ and 260 K (sample 3). The small hysteresis (within the measurement uncertainties) is taken as evidence that chemical reaction is negligible compared with the physical gating effect. The accumulation time is 800 s.

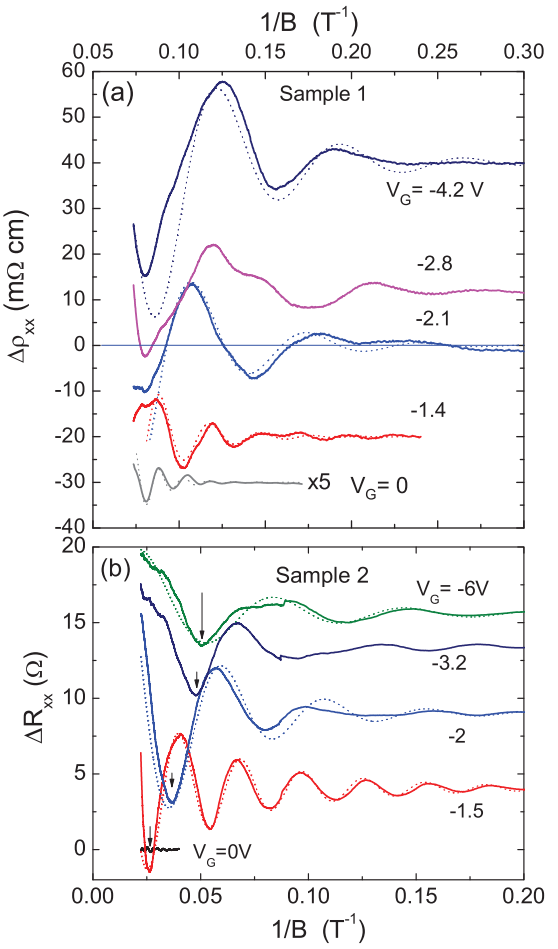

FIG. 3. (Color online) Traces of SdH oscillations in resistance versus $1/B$, showing systematic changes to the oscillation amplitude and period with gate voltage (bold curves, displaced vertically for clarity). Dashed curves are fits to the Lifshitz-Kosevich expression with one frequency component.[11] (a) Traces of $\Delta\rho_{xx}$ vs $1/B$ at 5 K measured to 14 T for five values of V_G (sample 1). The largest increase in amplitude occurs between $V_G = 0$ and $V = -1.4$ V. The curve at $V_G = 0$ is shown amplified 5×. All other curves share the same vertical scale. (b) Traces of ΔR_{xx} vs $1/B$ at 1.6 K measured to 45 T at V_G as indicated (sample 2). Arrows indicate $n = \frac{1}{2}$ (E_F at center of broadened $N = 1$ LL).

LLs (the highest filled LL has $N_{\max} = n - 1$). Using the level degeneracy Be/h per spin, we then have $1/B_n = ne/(hn_s)$ (n_s is the surface density, e is the elemental charge, and h is Planck's constant).

For Dirac electrons, however, we have $n + \frac{1}{2}$ filled LLs when $B = B_n$ (now $N_{\max} = n$). The additional $\frac{1}{2}$ derives from the $N = 0$ LL or, equivalently, from the π-Berry phase intrinsic to each Dirac cone.[21] The relation between $1/B_n$ and n is now $1/B_n = (n + \frac{1}{2})(e/hn_s)$—a straight line that intercepts the n axis at $n = -\frac{1}{2}$. In both cases, G_{xx} is a local minimum at B_n.

If resistivity curves are used, B_n should be identified with the *maxima* in $\Delta\rho_{xx}$. This point is discussed in Refs. 11 and 22. In Fig. 4(a), we plot as filled symbols B_n in sample 1 against the integers n (the open symbols corresponding to the minima are plotted vs $n + \frac{1}{2}$).

At each V_G, the slope of the straight lines yields the FS area S_F. As $|V_G|$ increases from 0 to 2.8 V, the slopes of the best-fit lines decrease by a factor of 6.4, reflecting a steep decrease in S_F. This decrease saturates when $|V_G|$ exceeds 2.1 V.

In Fig. 4(b), we show the high-field behavior for $|V_G| >$ 2.1 V on an expanded scale. At these large bias values, the intercepts cluster around $n = -\frac{1}{2}$ (-0.46, -0.56, and -0.61). In the corresponding plots for sample 2 [Fig. 4(c)], we find that S_F decreases by a factor of 2 between $V_G = -1.4$ and $V_G + -6$ V. In the limit $1/B \to 0$, the intercepts are at $n = -0.35, -0.40$, and -0.42. In both samples, the last feature observed at the highest B (minima in R_{xx}) corresponds to $n_{\min} = \frac{1}{2}$ [as shown in the inset in Fig. 4(b), this implies that E_F lies in the middle of the broadened $N = 1$ Dirac LL]. With such a small $n_{\min}$, we may rigorously exclude an intercept at $n = 0$ in the limit $1/B \to 0$.[22] Thus the index plots provide rather conclusive evidence that the SdH oscillations arise from surface Dirac fermions.

The ability to reach $n = \frac{1}{2}$ is important for experimentally determining the Berry phase π shift. Because the surface SdH oscillations are generally very weak (for $B < 14$ T), there is considerable uncertainty in determining the intercept in the limit $1/B \to 0$ if the lowest n achieved at the maximum

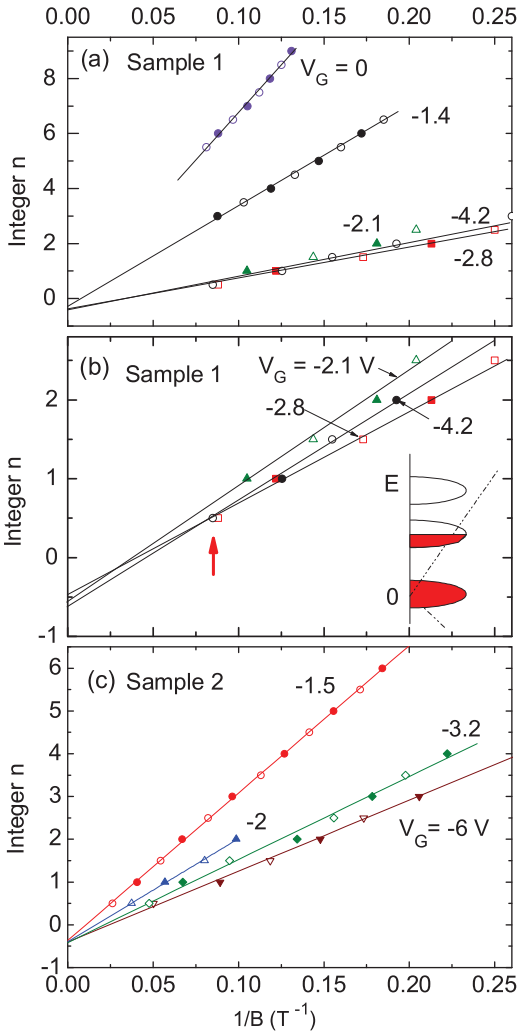

FIG. 4. (Color online) Index plots of the integer n vs $1/B_n$ at selected V_G in sample 1 (a), (b) and sample 2 (c). Maxima of $\Delta\rho_{xx}$ (filled symbols), corresponding to the index fields B_n, are plotted against n. Minima (open symbols) are plotted vs $n+\frac{1}{2}$. (a) As V_G changes from 0 to -2.1 V, the slope of the best-fit lines decreases sixfold. Further increase in $|V_G|$ leads to saturation. (b) High-bias curves are displayed on an expanded vertical scale. In the limit $1/B \to 0$, the best-fit lines have intercepts at -0.46, -0.56, and -0.61, consistent with Dirac fermions. The datum at $n=-\frac{1}{2}$ (arrow) corresponds to E_F sitting in the middle of the broadened $N=1$ LL (inset). (c) The intercepts for sample 2 also cluster near -0.45 in the limit $1/B \to 0$.

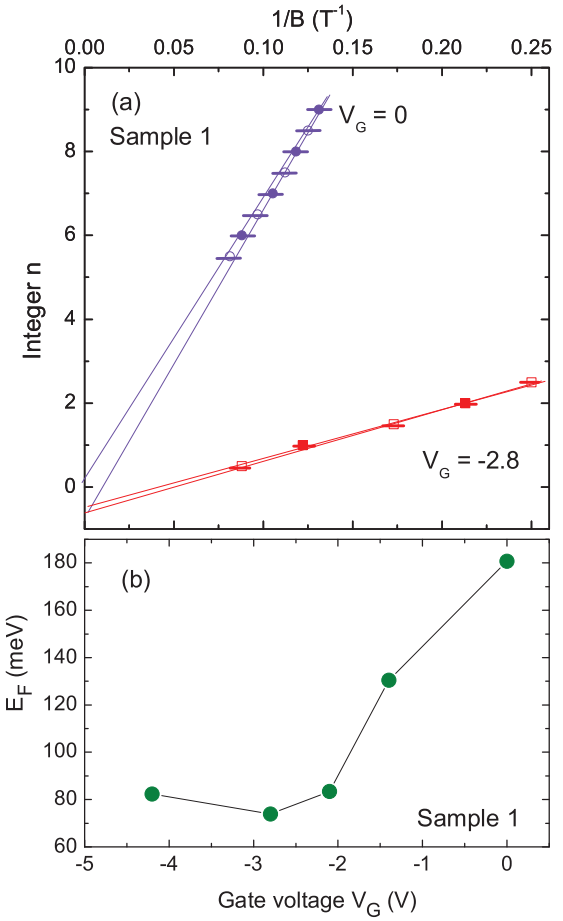

FIG. 5. (Color online) (a) Comparisons of extrapolations of index plot to the limit $1/B \to 0$ for index fields measured with $V_G=0$ (circles) and measured with $V_G=-2.8$ V (squares) in sample 1. (b) Variation of E_F with applied V_G in sample 1 (E_F is measured from the Dirac point). The FS cross section S_F is converted to E_F by $E_F=\hbar v\sqrt{S_F/\pi}$ using $v=6\times10^5$ m/s.[9] For $|V_G|>2$ V, the decrease in E_F saturates.

available B is 5 or larger. We illustrate the uncertainties incurred in Fig. 5(a). In the absence of gating ($V_G=0$), the uncertainties δB_n in measuring the index fields are typically $\pm5\%$ (circles). As shown, this yields a considerable spread in the allowed intercepts (the lowest datum corresponds to $n=5.5$). For comparison, at the gate voltage $V_G=-2.8$ V (squares), the lowest datum corresponds to $n=\frac{1}{2}$. This tightens up considerably the spread in the allowed intercepts. The same advantage may be achieved by applying an intense B (45 T), as done in Ref. 11.

For convenience, we have converted the values of S_F inferred from the slopes of the index plots in Figs. 6(a) and 6(b) to the Fermi energy $E_F=\hbar v\sqrt{S_F/\pi}$ using the Fermi velocity $v=6\times10^5$ m/s.[9] The variation of E_F vs V_G in sample 1 [Fig. 5(b)] shows that E_F decreases by 100 mV as V_G is changed from 0 to -2 V. Thereafter, it remains at $\sim$80 mV. This is used below to estimate the depletion capacitance. We remark that E_F stops decreasing when $|V_G|$ exceeds 2 V. Since the Dirac point is close to the top of the valence band, we do not reach the limit of band inversion (which would lead to an accumulation layer of holes) in this experiment.

Returning to Fig. 3, we have fitted the SdH oscillations to the Lifshitz-Kosevich expressions (shown as dashed curves). The damping of the oscillations versus B yields the surface mobility μ_s. As shown in Fig. 6(b), μ_s in sample 1 rises from 720 to 2480 cm^2/V s as $|V_G|$ is increased to 4.2 V. In Fig. 6(c), the decrease and eventual saturation in S_F are plotted as a surface density $n_s=k_F^2/(4\pi)$ (per spin). The saturation at large $|V_G|$ arises either from induced chemical reaction or from E_F meeting the top of the valence band.

One figure of merit in TI crystals is the ratio of the surface to bulk conductances $\eta\equiv G^s/G^b$ in zero B [with $G^r\equiv G^r_{xx}(0)$, $r=s,b$]. In sample 1, $\eta\sim0.05$ is quite small (compared with the $\eta\sim1$ obtained in Ref. 9). However, in the Hall channel,

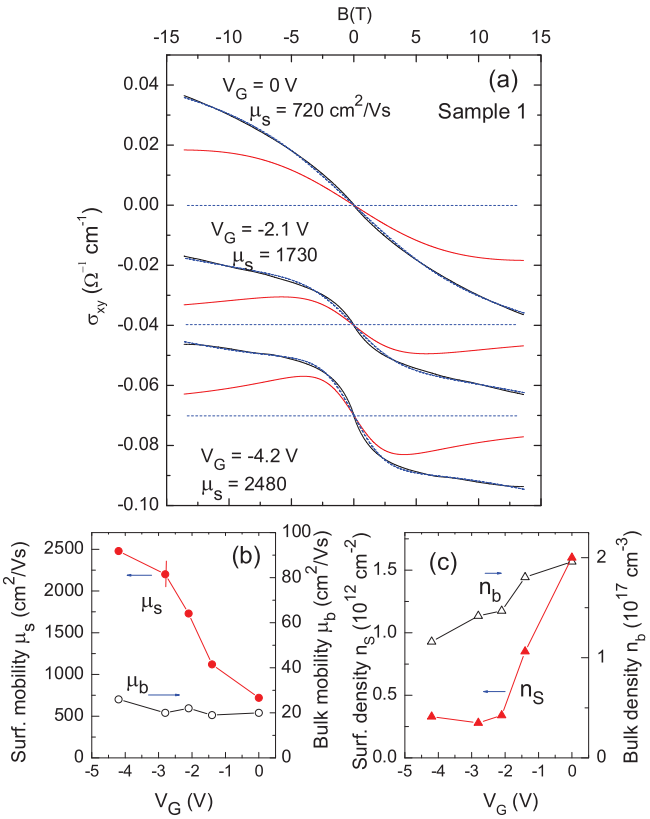

FIG. 6. (Color online) (a) Observed Hall conductivity σ_{xy} vs B in sample 1, showing weak-B curvature at three values of V_G (curves displaced, for clarity). At each V_G, the outer curves are the data [solid (black) curve] and the fit to Eq. (1) [dashed (blue) curve]. The inner [solid (red)] curve is the surface term G^s_{xy}/t fixed by n_s and μ_s. The difference between the outer and the inner curves is the bulk term σ^b_{xy}. At $V_G = -4.2$ V, G^s_{xy}/t accounts for 83% of σ_{xy} in weak B. (b) With increased gating, μ_s increases from 720 to 2480 cm^2/V s, while μ_b stays very small (20–30 cm^2/V s). (c) Comparison of the sharp decrease in n_s with the mild change in n_b with gating. When $|V_G| > 2$ V, n_s saturates.

the ratio $\eta_H = G^s_{xy}/G^b_{xy}$ of the surface and bulk conductances (G^s_{xy} and G^b_{xy}, respectively) is enhanced by μ_s/μ_b, which can be very large. We define n_b and μ_b to be the bulk electron density and mobility, respectively, averaged over the whole crystal.

As shown in Fig. 6(a), a distinctive feature of σ_{xy} at low T is the curvature in weak B, which grows with increasing $|V_G|$. We may use the semiclassical two-band expression for σ_{xy},

$$\sigma_{xy} = n_s e\mu_s \frac{\mu_s B}{t[1+(\mu_s B)^2]} + n_b e\mu_b^2 B, \qquad (1)$$

where the first term is G^s_{xy}/t, with t the thickness (50 μm in sample 1). With n_s and μ_s fixed by analysis of the SdH oscillations, this term is nonadjustable. The second term is the bulk Hall conductivity σ^b_{xy} in the low-mobility limit. With the sole adjustable parameter $P_b \equiv n_b\mu_b^2$, we find that Eq. (1) gives a very good fit (dashed curves). For comparison, we have also plotted G^s_{xy}/t (inner, faint solid curves). Combining P_b with the zero-B value of σ^b_{xx}, we finally obtain n_b and μ_b separately for each value of V_G. These are reported in Figs. 6(b) and 6(c). The small values of μ_b (20–30 cm^2/V s) result in a large $\mu_s/\mu_b \sim 100$ and $\eta_H \sim 5$. This accounts for the pronounced low-B curvatures shown in Fig. 6.

The analysis implies high-mobility Dirac electrons in parallel with a much larger population of bulk electrons. Because of the 100-fold difference in mobilities, the Dirac electrons produce 83% of the total weak-B Hall conductance at large $|V_G|$. The fits include the surface Hall conductance from only one surface. Since its G^s_{xy} already accounts for most of the observed σ_{xy}, there is very little room left for a second surface term. We estimate that the Hall contribution from the other surface is less than 2% of σ_{xy}, which implies that its μ_s is <300 cm^2/V s. This cannot produce resolvable SdH oscillations.

IV. DEPLETION-LAYER CAPACITANCE, SCREENING, AND IMPURITY BAND

Our main results are on the tuning of the SdH oscillations of the Dirac surface states. However, the experiment also yields quantitative results on the electronic parameters in the depletion region, which provide a detailed picture of what happens under liquid gating. A useful feature of the experiment is that, at each value of the applied gate voltage V_G, we can measure via the SdH oscillations both n_s and E_F of the surface carriers [hence the surface electrostatic potential $\varphi(0)$]. In addition, we measure the carrier density and conductivity of the bulk carriers and the anion charge Q accumulated on the crystal surface. The five quantities provide a detailed picture of the band-bending process as well as self-consistency checks in determining the depletion capacitance. We apply the standard analysis of field-effect gating,[25–27] which is summarized in Appendix B.

For gating to induce band bending, the chemical potential must already lie inside the bulk gap in zero V_G (the case for Bi_2Te_2Se). [If, instead, E_F lies high in the conduction band (as is the case in as-grown Bi_2Se_3), the applied E field leads to Thomas Fermi screening[26] for which the screening length $\lambda_{TF} = \sqrt{\pi a_B/4k_F}$ is typically a few angstroms ($a_B = \hbar^2/me^2$ is the Bohr radius)]. For a hard gap (impurity band absent), a negative V_G leads to a depletion region. However, despite displaying a very high bulk resistivity (2–6 Ωcm) at 4 K, the current generation of Bi_2Te_2Se crystals still has a substantial bulk carrier density ($n_b \sim 2\times10^{17}$ cm^{-3}). This implies that an impurity band extends across the gap. Nonetheless, band bending over a significant depletion region ($\sim$10 μm) is observed. We analyze this situation at the end of this section, after we estimate the depletion capacitance (see also Appendix A).

For $V_G < 0$, the E field from the anions repels bulk electrons away from the surface, exposing the ionized donors within the depletion width d. Figure 7(a) shows a sketch of the band bending near the surface exposed to the liquid. For finite V_G, the ionic liquid polarizes to form, in effect, two capacitors, each with spacing of the order of the molecular radius a. Each capacitor stores the charge Q. The capacitor at the gate electrode has an area A' much larger than that of the capacitor at the crystal surface A, so that most of the potential drop $V_G - V_s$ falls across the latter [V_s is the voltage corresponding to $\varphi(0)$ and the ground is taken deep in the bulk

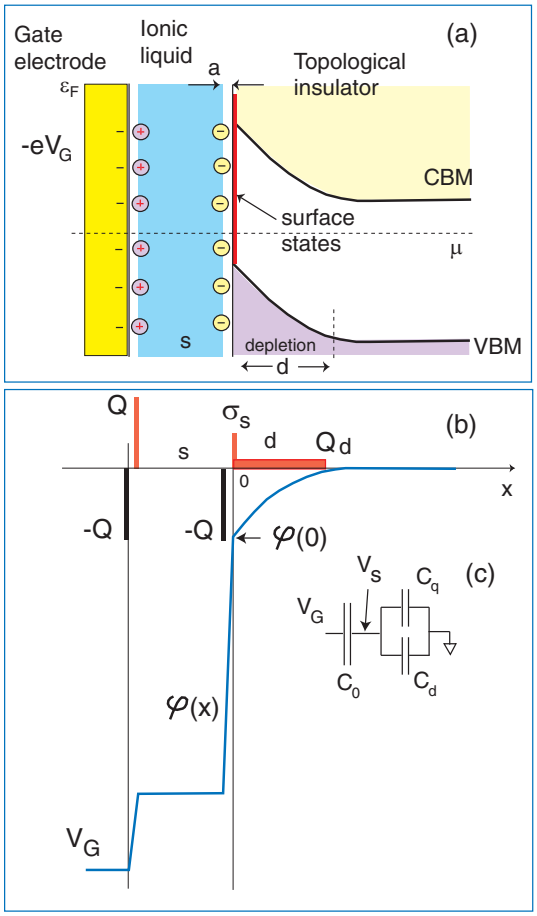

FIG. 7. (Color online) Sketch of band bending and profiles of $\rho(x)$ and $\varphi(x)$ in the liquid gating experiment. (a) Upwards bending of the bands induced by a negative gate voltage V_G. The cations and anions define two series capacitors with spacing a (molecular radius). The depletion layer in the bulk of the TI extends a distance d. (b) Charge distribution versus x. The negative charge $-Q$ on the gate electrode is replicated by the anion layer separated by a from the TI surface. This is compensated by the sum of the surface charge density σ_s and the ionized impurity charges inside the depletion layer [Eq. (A8)]. The electric potential $\varphi(x)$ corresponding to $\rho(x)$ is sketched. (c) Circuit of the equivalent capacitors C_0, C_d, and C_q.

at $x \to +\infty$]. In sample 1, $A = 2.9$ mm^2 and $A' = 30$ mm^2. The E field produced by the anion layer just to the left of the crystal surface is $E(0^-) = Q/A\epsilon_0$.

In Fig. 7(b), we sketch the profiles of the charge density $\rho(x)$ and the electrostatic potential $\varphi(x)$ (the x axis is normal to the surface). Within the liquid, the charge densities of the cations and anions are taken to be δ functions of strength $\pm Q$. In the TI, the surface charge density is represented by a δ function (σ_s). Within the bulk, however, $\rho(x)$ is distributed over the depletion layer to a depth d. As a guide, it is convenient to adopt the usual approximation, whereby $\rho(x)$ is taken to be uniform for $0 < x < d$. In the uniform-charge approximation, $\varphi(x)$ varies as $-(x-d)^2$ in the depletion region. Its value at the surface is then

$$\varphi(0) = -N_d e d^2/(2\epsilon_0\epsilon_s), \qquad (2)$$

where N_d is the donor impurity concentration and ϵ_s the screening dielectric parameter. The charge Q_d induced in the depletion width by $\varphi(0)$ defines the depletion capacitance $C_d = N_d e d A/\varphi(0) = \epsilon_0\epsilon_s A/d$. The surface charge density σ_s induced by $\varphi(0)$ is represented by the quantum capacitance $C_q = \sigma_s/\varphi(0) = e^2(dn_s/d\mu)$. Clearly, C_d and C_q are in parallel combination [Fig. 7(c)].

The large slope change in $\varphi(x)$ at $x = 0$ mainly reflects the strong dielectric screening in the bulk of the TI (σ_s makes a negligible contribution). Thus the intense E field produced by the anions is strongly screened by polarization effects inside the crystal [$E(0^-) \gg E(0^+)$]. As shown in Fig. 7(c), the parallel combination of C_d and C_q is in series with C_0, the series combination of the cation and anion capacitances. In all samples, we find that $C_d \gg C_q$, so we may ignore the quantum capacitance in the discussion below.

A. Magnitude of C_d

As shown in Fig. 5(b), E_F in sample 1 decreases by $\sim$100 mV when the applied V_G is -2 V. Thus, only a small fraction ($\sim$1/20) of the applied gate voltage is effective in bending the band ($V_s = -0.1$ V). We can use this observation to determine the depletion capacitance C_d. The value of C_0/A for ionic liquids is 11–12 μF/cm^2.[28] (From the expression $C_0/A = \epsilon_0\epsilon_{\rm liq}/a$, this corresponds to $\epsilon_{\rm liq} = 4$, and $a = 3$ Å.) Using the ratio $V_s/(V_G - V_s) \sim C_0/C_d$ (neglecting C_q), we estimate that $C_d/A \simeq 240$ μF/cm^2.

Alternatively, we may estimate C_d by integrating the ionic current to find the charge Q. For sample 1 with $V_G = -2$ V, the ionic charge current deposits a total negative ionic charge at the surface equal to $-Q/A \sim 2 \times 10^{14}$ e/cm^2 $= -3.2 \times 10^{-5}$ C/cm^2. Since Q/A is stored in C_d by the voltage $V_s \sim 0.1$ V, we have $C_d/A \sim 320$ μF/cm^2, which is 33% larger than the first estimate, but within our uncertainties. The main source of uncertainty is the actual area coated by the anions. Because the ions can coat the silver paint contacts and voltage and current leads, the area can exceed that of the crystal A by 50% to 100%.

(By equating Q/A to $N_d e d$ [see Eq. (A8)], we may estimate the depletion width d as a check. The donor density N_d is roughly equal to the bulk density observed at 4 K, $n_b \sim 2 \times 10^{17}$ cm^{-3}. This gives $d \simeq 10$ μm. The deep penetration of the depletion region into the bulk is consistent (within a factor of 2) with the 40% change observed in the resistivity and Hall coefficient at 4 K.)

Taking the range $C_d/A = 240$–320 μF/cm^2, we find that the depletion capacitance is 5000–6000$\times$ larger than the values commonly observed in a Si-MOSFET device ($C_{d,Si}/A \simeq 0.05$–0.06 μF/cm^2).[25,27] The enhancement points to a very large polarizability in the ground state of Bi_2Te_2Se when E_F lies inside the energy gap. This is perhaps unsurprising given that the energy gap in high-purity Si is devoid of impurity states. By contrast, Bi_2Te_2Se at 4 K displays a low, but metallic conductivity arising from a large population of impurity-band electrons.

Here, we resume discussion of the finite density of states (DOS) in the gap. To create an extended depletion region with significant band bending, as we have here [Fig. 7(a)], the weak bulk conductivity must be further driven to zero

throughout the depletion region in order to sustain a finite E field (otherwise one has Thomas Fermi screening with the very short screening length $\lambda_{TF} \simeq 6$ Å for $n_b = 2 \times 10^{17}$ cm^{-3}m). To explain how band bending is sustained over a large depletion region, we need the existence of a mobility edge in the impurity band. Throughout the depletion layer, E_F lies below the mobility edge so that the conductivity is vanishingly small at 4 K. Because impurity-band states close to the mobility edge have a greatly enhanced polarizability in an E field, we expect the electronic contribution to the dielectric constant ϵ_s to be orders of magnitude larger than the lattice contribution. Measurements of C_d/A probe directly the electronic polarizability in the depletion region. A possible scenario is described in Appendix B and Fig. 11.

V. CONCLUSIONS

Applying the technique of ionic liquid gating to bulk crystals of Bi_2Te_2Se with resistivity exceeding 4 Ωcm at 5 K, we find that E_F of the surface Dirac fermions can be tuned over a considerable range. In contrast to previous gating experiments, we readily resolve the surface SdH oscillations at each value of the gate voltage. By measuring the SdH period, we find that the surface Fermi energy E_F (Sample 1) decreases from 180 mV to 75 mV relative to the Dirac point as V_G is changed from 0 to −2.8 V. In a field of 14 T, the lower limit corresponds to the middle of the broadened $N = 1$ LL. Reaching such low LLs enables the $-\frac{1}{2}$ intercept (predicted for Dirac fermions) to be determined with high accuracy. We also find that the intercepts are closely similar for a broad range of V_G in both sample 1 and sample 2.

Using the surface mobility μ_s and density n_s determined from the SdH oscillations, we find that the Dirac fermion Hall conductivity from the surface exposed to the anions accounts for up to 83% of the total observed weak-B Hall conductivity at 5 K. The analysis allows an accurate determination of the bulk carrier mobility and density at each V_G (Fig. 6). The picture inferred is that, with gating, the density n_s of the surface Dirac fermions decreases steeply, while their mobility μ_s increases to a maximum value of 2400 cm^2/V s. The bulk carriers are depleted to a depth of 10 μm from the surface, with μ_b remaining at the low value 20 cm^2/V s.

The large enhancement of μ_s by liquid gating [Fig. 6(b)] is perhaps the most intriguing feature reported here. To our knowledge, this is the first realization of enhancement of surface SdH amplitudes by an *in situ* technique.[23] A recent STM experiment[24] reveals that the Dirac point closely follows spatial fluctuations of the local potential on length scales of 30–50 nm. This could lead to strong scattering of surface electrons. We speculate that, under liquid gating, the anions accumulate at local maxima in the potential, thereby leveling out the strongest spatial fluctuations. The results provide encouragement that alternative routes that even out local potential fluctuations can lead to further improvements in μ_s.

To address the question whether ionic liquid gating actually alters the carrier concentration by chemical reaction (as opposed to simply bending the band), we have performed extensive tests to separate the two effects. By carefully selecting the experimental conditions (e.g., the gating temperature), monitoring charge accumulated Q, and checking for reversibility, we establish that band bending is the dominant effect in these experiments. Finally, the five quantities measured at each gate voltage setting (E_F, n_s, n_b, ρ, and Q) provide a quantitative picture of the gating process. The depletion capacitance measured implies that, within the depletion region, the electronic polarizability is strongly enhanced.

ACKNOWLEDGMENTS

We thank Joe Checkelsky, Jianting Ye, and Hongtao Yuan for advice on liquid gating. The research was supported by the Army Research Office (ARO W911NF-11- 1-0379) and by the US National Science Foundation (Grant No. DMR 0819860). Sample growth and characterization were supported by an award from the Defense Advanced Research Projects Agency under SPAWAR Grant No. N66001-11-1-4110. High-field measurements were performed at the National High Magnetic Field Laboratory, which is supported by the NSF (Award No. DMR-084173), by the State of Florida, and by the Department of Energy.

APPENDIX A: GATING TEMPERATURE

We discuss here the factors that dictate our choice of the "gating" temperature. Insight on the ion accumulation process is provided by monitoring the transient current I_{trans} following a step change in V_G (with T fixed in the interval $208 < T < 260$ K). As the ions flow to adjust to the new potential, $I_{trans}(t)$ decays over a time scale of 10^3 s. As shown in Fig. 8, $I_{trans}(t)$ fits well to the stretched exponential form,

$$I_{trans}(t) = I_0 e^{-(t/\tau)^\alpha} + I_b, \tag{A1}$$

where α varies from 0.35 to 0.50 depending on T, and I_b is the long-term, steady-state background current. Integrating the transient part, we obtain the ionic charge accumulated at time t, $Q(t) = \int_0^t dt'[I_{trans}(t') - I_b]$.

In our experiment, the optimal temperature falls in the window 220–240 K. As shown in Fig. 8, the background I_b is

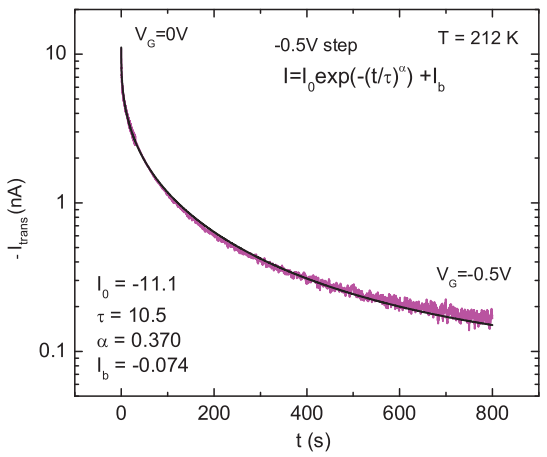

FIG. 8. (Color online) Transient (discharging) current I_{trans} versus time t following a step change of V_G from 0 to −5 V at $t = 0$ at $T = 212$ K in sample 3. The observed current fits well to the stretched exponential form Eq. (A1) with the parameters $I_0 = -11.1$ nA, $I_b = -0.074$ nA, $\alpha = 0.37$, and $\tau = 10.5$ s. I_b is the long-term steady-state background current.

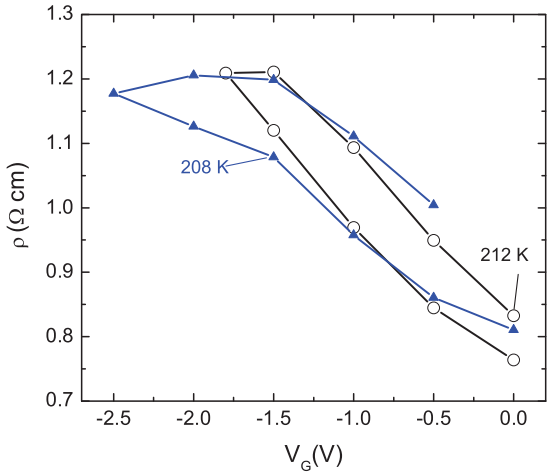

FIG. 9. (Color online) Apparent hysteretic behavior of ρ vs V_G observed at temperatures close to the glass transition T_G. Varying V_G at T too closely to T_G strongly suppresses the background quasi–steady state I_1 and possibilities of chemical reaction. However, this imparts increased hysteresis in ρ when V_G is cycled (here $T = 208$ and 212 K). The Hall density n_H shows similarly large hysteresis (not shown). As discussed in the text, we show that this apparent low-temperature hysteresis results from incomplete melting of the ionic liquid.

a factor of 10–100 smaller than the onset value I_0. Raising T above 240 K leads to an exponential increase in I_b. Most of this arises from the finite (if small), thermally activated bulk conductivity of the ionic liquid. In addition, chemical reaction adds an increasingly important component to I_b when $|V_G|$ exceeds 2 V. For these reasons, we keep T under 240 K.

To minimize possible chemical reaction, it might seem expedient to lower the gating T to as close to the glass transition as feasible (this strongly suppresses I_b). However, we quickly encounter a different problem, namely, the failure of the ionic charge configuration to melt completely. As a result, $Q(t)$ fails to attain its equilibrium value as V_G is changed (even if $t \gg 10^3$ s), leading to a different kind of hysteresis.

Figure 9 plots the changes in ρ (sample 3) as V_G is cycled between 0 and −2.5 V at a relatively low T (208 and 212 K). In contrast to Fig. 2, we observe sizable hysteretic behavior (also in n_H; not shown). To show that this is not caused by chemical reaction (which should be greatly suppressed at low T), we have measured the accumulated $Q(t)$ and found that it displays the same hysteresis (vs V_G). When we plot the changes in ρ and n_H vs $n_{\rm ion} = Q/eA$ (see Fig. 10), the hysteretic behavior apparent in Fig. 9 is largely removed.

This implies that, at these low T, a significant portion of the ionic "solid" accumulated at the previous value of V_G fails to melt and flow in response to the new V_G. Hence $Q(t)$ never attains its equilibrium value even at long t. This leads to strong hysteresis in Q vs V_G. However, the near-absence of hysteresis in Fig. 10 shows that ρ and n_H adjust reversibly to the nonequilibrium value of Q. The key parameter that causes ρ and n_H to change is the electric field $E(0^-)$ produced by Q even when it lags the applied V_G. This direct link provides further support for our conclusion that the dominant effect of changing Q is band bending.

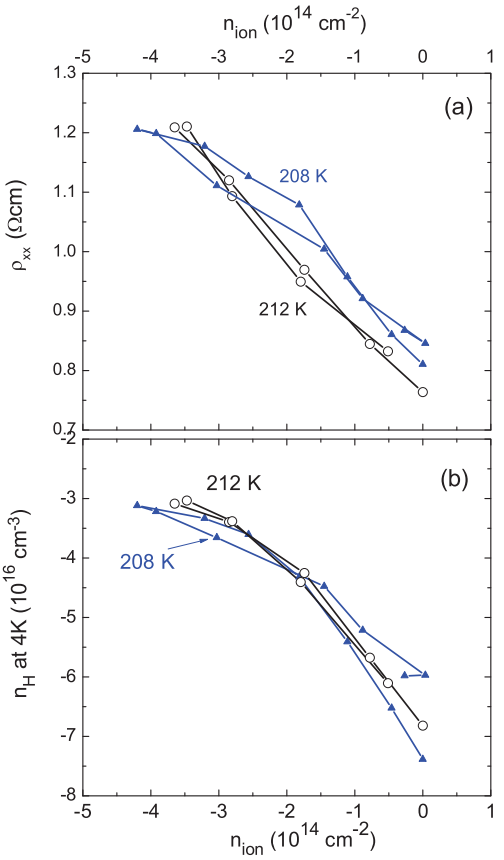

FIG. 10. (Color online) Absence of low-temperature hysteresis when ρ and n_H are plotted against $n_{\rm ion} = Q/eA$, with $A = 2.9$ mm^2. Replotting the data for ρ in Fig. 9 versus $n_{\rm ion}$ (instead of V_G) removes the hysteresis apparent in Fig. 9. This shows that the hysteretic behavior arises from the variation of Q vs V_G. The physically relevant quantities inside the crystal ρ and n_H are dependent only on Q, strongly supporting the premise that band bending produces these changes rather than chemical reaction.

APPENDIX B: DEPLETION AND QUANTUM CAPACITANCES

With reference to Fig. 7, the free-charge density profile $\rho(x)$ is comprised of four δ functions $\delta(x)$ and an extended distribution over the depletion width d [which we assume has a flat profile expressed by the step function $\theta(x)$,[26] as shown in Fig. 7(b)]. Setting the origin $x = 0$ at the TI surface, we have

$$\rho(x) = -\frac{Q}{A'}\delta(x+s) + \frac{Q}{A'}\delta(x+s-a) - \frac{Q}{A}\delta(x+a) + \sigma_s\delta(x) + N_d e d\,[\theta(x) - \theta(x-d)], \tag{A2}$$

where σ_s is the surface charge density at the exposed crystal face, and N_d is the density of ionized donor impurities within the depletion width d (we take $e > 0$). The electrostatic potential $\varphi(x)$ is derived from the Poisson equation,

$$-\varepsilon(x)\frac{\partial^2\varphi}{\partial x^2} = \frac{\rho(x)}{\epsilon_0}, \tag{A3}$$

with ϵ_0 the vacuum permittivity. The dielectric function $\varepsilon(x) = \epsilon_s$ inside the TI ($x > 0$). Within the ionic liquid, $\varepsilon(x) = \epsilon_{\rm liq}$.

Integration of Eq. (A3) gives the profile of $\varphi(x)$ sketched in Fig. 7(b). We wish to relate the charge density Q/A to σ_s

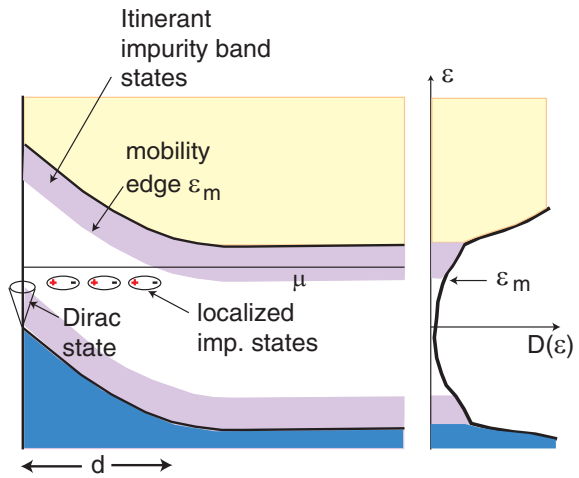

FIG. 11. (Color online) Model for the impurity band states implied by the liquid-gating experiment. The density of states (DOS) profile $\mathcal{D}(\varepsilon)$ across the bulk energy gap is sketched at the right. The impurity-band DOS tapers deep into the gap, as suggested by STM experiments.[24] Impurity states lying above the mobility edge ε_m (shaded) are itinerant, with mobility $\mu_b \sim 20$ cm^2/V s. States below ε_m are strongly localized at 4 K. Near the surface (left), ε_m is lifted above μ within the depletion layer, substantially decreasing the bulk contribution to the observed σ and σ_H. Localized states near the mobility edge (sketched as dipoles) contribute strongly to dielectric screening because of their enhanced polarizability.

and d. Setting φ and $\partial\varphi/\partial x$ to 0 deep in the bulk ($x > d$), we have for the E-field just to the right of $x = 0$

$$E(0^+) = -\left(\frac{\partial\varphi}{\partial x}\right)_{0+} = -\frac{N_d e d}{\epsilon_0 \epsilon_s}. \tag{A4}$$

In the flat-profile approximation for $\rho(x)$, Eq. (A3) gives the parabolic variation of $\varphi(x)$:

$$\varphi(x) = -\frac{N_d e}{2\epsilon_0 \epsilon_s}(x-d)^2 \quad (x > 0). \tag{A5}$$

Next, we integrate Eq. (A3) between the limits $x = 0^{\pm}$ (bracketing $x = 0$) to get

$$\epsilon_s E(0^+) - E(0^-) = \sigma_s/\epsilon_0. \tag{A6}$$

Together, Eqs. (A4) and (A6) give, for the E field just to the left of the surface,

$$E(0^-) = -(\sigma_s + N_d e d)/\epsilon_0. \tag{A7}$$

This strong E field emanating from the anion charge $-Q$ is only partially screened by the surface charge σ_s. The remaining E penetrates a distance d into the bulk until screened by enough ionized donor charge. The lattice polarizability, expressed by the bulk dielectric constant ϵ_s, also contributes to the screening. [It is helpful to represent the dielectric screening, alternatively, as a bound-surface charge density $\sigma_b = -\epsilon_0(\epsilon_s - 1)E(0^+)$ at $x = 0$. However, this bound charge should not be included in $\rho(x)$.]

Finally, identifying $E(0^-)$ with the E field within the molecular layer, $-Q/A\epsilon_0$, we arrive at the equation

$$\frac{Q}{A} = N_d e d + \sigma_s. \tag{A8}$$

We note that Eq. (A8) is independent of ϵ_s. The charge Q induced by the anions is partitioned between two charge reservoirs, which see the same potential drop, $V_s = \varphi(0)$, relative to the ground at $x = +\infty$. Hence, as shown in Fig. 7(c), we regard the two charge reservoirs as two capacitors in parallel, namely, the quantum capacitance,[29]

$$C_q = \frac{\sigma_s}{\varphi(0)} = e^2 \frac{dn_s}{d\mu}, \tag{A9}$$

and the depletion-layer capacitance,

$$C_d = N_d e d A/\varphi(0). \tag{A10}$$

Whereas in graphene, the quantum capacitance is readily resolved, here it is shunted by the large C_d.

The parallel combination $C_q + C_d$ is in series with the ionic-liquid capacitor C_0 (the series combination of the cation and anion capacitors). The voltage drop across C_0 is $V_G - V_s$.

1. Mobility edge and electronic polarizability

We discuss a scenario in which a strongly enhanced electronic polarizability arises within the depletion layer. Figure 11 is a sketch of the band bending near the surface. As shown, the chemical potential μ in the bulk lies just below the bottom of the conduction band. The right sketch plots the DOS $\mathcal{D}(\varepsilon)$ in a cut in the bulk. The impurity band is comprised of "tails" of $\mathcal{D}(\varepsilon)$ which taper downwards (upwards) from the conduction band (valence band).[24] At 4 K, the mobility edge ε_m sharply divides states that are itinerant (closer to the gap edge) from states that are localized. Electrons in the itinerant states diffuse with the observed mobility $\mu_b \sim 20$ cm^2/V s. In an E field strong enough to cause band bending, ε_m is lifted above μ within the depletion region of width d. Occupied states within this region are strongly localized, so they do not contribute to the observed conductivity or Hall effect. However, because the localization length $\xi_{\rm loc}$ diverges as $\varepsilon \to \varepsilon_m$ from below, the localized states have a greatly enhanced electronic polarizability. The electronic component of the dielectric screening parameter will be much larger than that from the lattice polarizability.

[1] M. Z. Hasan and C. L. Kane, Rev. Mod. Phys. **82**, 3045 (2010).
[2] X.-L. Qi and S.-C. Zhang, Rev. Mod. Phys. **83**, 1057 (2011).
[3] D. Hsieh, D. Qian, L. Wray, Y. Xia, Y. S. Hor, R. J. Cava, and M. Z. Hasan, Nature (London) **452**, 970 (2008).
[4] P. Roushan, J. Seo, C. V. Parker, Y. S. Hor, D. Hsieh, D. Qian, A. Richardella, M. Z. Hasan, R. J. Cava, and A. Yazdani, Nature (London) **460**, 1106 (2009).
[5] D.-X. Qu, Y. S. Hor, J. Xiong, R. J. Cava, and N. P. Ong, Science **329**, 821 (2010).

[6]J. G. Analytis, R. D. McDonald, S. C. Riggs, J.-H. Chu, G. S. Boebinger, and I. R. Fisher, Nature Phys. **6**, 960 (2010).
[7]H. Peng, K. Lai, D. Kong, S. Meister, Y. Chen, X.-L. Qi, S.-C. Zhang, Z.-X. Shen, and Y. Cui, Nat. Mater. **9**, 225 (2009).
[8]Z. Ren, A. A. Taskin, S. Sasaki, K. Segawa and Y. Ando, Phys. Rev. B **82**, 241306(R) (2010).
[9]J. Xiong, A. C. Petersen, D. Qu, Y. S. Hor, R. J. Cava, and N. P. Ong, Physica E **44**, 917 (2012).
[10]S. Jia, H. W. Ji, E. Climent-Pascual, M. K. Fuccillo, M. E. Charles, J. Xiong, N. P. Ong, and R. J. Cava, Phys. Rev. B **84**, 235206 (2011).
[11]J. Xiong, Y. Luo, Y. H. Khoo, S. Jia, R. J. Cava, and N. P. Ong, Phys. Rev. B **86**, 045314 (2012).
[12]J. G. Checkelsky, Y. S. Hor, R. J. Cava, and N. P. Ong, Phys. Rev. Lett. **106**, 196801 (2011).
[13]H. Steinberg, D. R. Gardner, Y. S. Lee, and P. Jarillo-Herrero, Nano Lett. **10**, 5032 (2010).
[14]B. Sacepe, J. B. Oostinga, J. Li, A. Ubaldini, N. J. G. Couto, E. Giannini, and A. F. Morpurgo, Nature Commun. **2**, 575 (2011).
[15]H. Steinberg, J.-B. Laloe, V. Fatemi, J. S. Moodera, and P. Jarillo-Herrero, Phys. Rev. B **84**, 233101 (2011).
[16]H. Yuan, H. Liu, H. Shimotani, H. Guo, M.i Chen, Q. Xue, and Y. Iwasa, Nano Lett. **11**, 2601 (2011).
[17]D. Kim, S. Cho, N. P. Butch, P. Syers, K. Kirshenbaum, S. Adam, J. Paglione, and M. S. Fuhrer, Nature Phys. **8**, 459 (2012).
[18]J. G. Checkelsky, J. Ye, Y. Onose, Y. Iwasa, and Y. Tokura, Nature Phys. **8**, 729 (2012).
[19]S. Shimizu1, R. Yoshimi, T. Hatano, K. S. Takahashi, A. Tsukazaki, M. Kawasaki, Y. Iwasa, and Y. Tokura, Phys. Rev. B **86**, 045319 (2012).
[20]K. Segawa, Z. Ren, S. Sasaki, T. Tsuda, S. Kuwabata, and Y. Ando, Phys. Rev. B **86**, 075306 (2012).
[21]Y. Zhang, Y.-W. Tan, H. L. Stormer, and P. Kim, Nature **438**, 201 (2005).
[22]In general, it is best to convert the resistivity tensor R_{ij} to the conductance tensor G_{ij} and to identify B_n with the minima in G_{xx}. However, in many experiments (two-terminal measurements or experiments on nanowires), the Hall resistance R_{yx} is unavailable. Because the total conductance in Bi-based TI systems is dominated by low-mobility bulk electrons, we have $|R_{yx}| \ll R_{xx}$. Then R_{xx} has a local maximum whenever G_{xx} has a local minimum, and we should identify B_n with the fields at which R_{xx} attains local *maxima*. The wrong assignment (identifying B_n with minima in R_{xx}) shifts the intercept by $\pm\frac{1}{2}$. This leads to misidentifying the SdH oscillations from bulk carriers as arising from Dirac electrons.
[23]Previous gating experiments reported either a decrease in μ_s with finite gating,[17] or a nonmonotonic variation of μ_s that trends downwards with increasing $|V_G|$.[20] SdH oscillations were not resolved in these studies.
[24]H. Beidenkopf, P. Roushan, J. Seo, L. Gorman, I. Drozdov, Y. S. Hor, R. J. Cava, and A. Yazdani, Nature Phys. **7**, 939 (2011).
[25]T. Ando, A. B. Fowler and F. Stern, Rev. Mod. Phys. **54**, 437 (1982).
[26]N. W. Ashcroft and N. D. Mermin, in *Solid State Physics* (Saunders College, Philadelphia, 1976), chap. 29.
[27]S. M. Sze, in *Physics of Semiconductor Devices* (John Wiley & Sons, New York, 1981), chap. 7.
[28]C. Nanjundiah, S. F. McDevitt, and V. R. Koch, J. Electrochem. Soc. **144**, 3392 (1997).
[29]S. Luryi, Appl. Phys. Lett. **52**, 501 (1988).